Journal of Advanced Joining Processes 3 (2021) 100046

Contents lists available at ScienceDirect

Journal of Advanced Joining Processes

journal homepage: www.elsevier.com/locate/jajp

Feasibility study on hybrid weld-bonded joints using additive manufacturing and conductive thermoplastic filament

M. Frascio [a,*], F. Moroni [b], E. Marques [c,d], R. Carbas [c,d], M. Reis [c], M. Monti [a], M. Avalle [a], L.F.M. da Silva [d]

[a] University of Genoa, Polytechnic School, via All' Opera Pia 15, 16145 Genoa, Italy
[b] Engineering and Architecture Department, University of Parma, Parco Area delle Scienze 181/A, 43124 Parma, Italy
[c] Instituto de Ciência e Inovação em Engenharia Mecânica e Engenharia Industrial (INEGI), Portugal
[d] Departamento de Engenharia Mecânica, Faculdade de Engenharia (FEUP), Universidade do Porto, Portugal

ARTICLE INFO

Keywords:
Joining
Polymers
Processing techniques
Numerical model
Adhesive bonding
Welding
FFF
Additive manufacturing AM

ABSTRACT

This work aims to explore innovative joining processes for additively manufactured components, and, in particular, to assess the feasibility of hybrid weld-bonded joints by comparing their performance with the baseline bonded and welded joint configurations. The novelty of the proposed solution lies in the fact that welding is achieved using a 3D printed material with conductive filaments, a solution derived from the use of embedded 3D printed circuits (direct printing) in the AM components. Direct printing can be used to obtain an accurate local control of the thermal cycle and to overcome geometrical limitations inherent to the process, as for example the need of access for the welding tools.

The feasibility of the hybrid weld-bonded joint was assessed and, while for adhesive bonding the use of dedicated surface treatments was found to be necessary to improve the joint performance, the welding process was determined to be the most promising joining process, especially when directly integrated into a multi material additive manufacturing (MMAM) process.

1. Introduction

New developments on Additive Manufacturing (AM) processes (Han and Lee, 2020, Tan et al., 2020) and the wider availability of high performance reinforced materials (Arif et al., 2020, van de Werken et al., 2020) are enabling new industrial AM applications, addressing the needs of various applications, including healthcare products (Ramola et al., 2019, Ghomi et al., 2020), robotics (Jilich et al., 2019, Kaur and Kim, 2019), light weight and safe vehicle structures (Zaharia et al., 2020, Özen et al., 2020) and, in general, where highly optimized-for-the-application components are used.

In particular, analysing the recent literature and the previously cited examples, it can be noticed that some of the most promising technology and design techniques advances are achieved by coupling the local control on the geometry (Mao et al., 2018, de Lima and Paulino, 2019), used for example to create field driven lattice structures, to the local control on the material properties provided by the multi-material processes, enabled by the widespread availability of materials with very different characteristics (Arif et al., 2020, Ahmed et al., 2020).

This design method belong to the Design for Additive Manufacturing (DfAM) concept (Alfaify et al., 2020) and one of DfAM aims is to integrate functions in the components geometry to achieve embedded multifunctionality Wood (2016) obtaining, for example, controlled stiffness or variable thermal and electrical conductivity (Wang et al., 2020).

Another focus of DfAM is that the widespread use of AM components creates a need for effective and practical joining processes, suitable to assemble these AM parts and create more complex final products.

Furthermore the nominally limitless design freedom, provided by the AM process features in some applications, could be not achievable due to the constrains of a 3D printer build volume, component positioning and 3D printing parameters adjusted for printability instead of maximum performance (Bardiya et al., 2020). This is especially true when service loads in structural applications require the use of AM with long fibre reinforced materials. Therefore, in many cases it is convenient to decompose the component in optimized sub-assemblies to enable the choice of the optimal printing set up for the application, using the effect of the print parameters on the material as design variable (Bergonzi et al., 2021, Frascio et al., 2019, Kiendl and Gao, 2020, Chacón et al., 2019)

* Corresponding author.
E-mail address: mattia.frascio@edu.unige.it (M. Frascio).

https://doi.org/10.1016/j.jajp.2021.100046
Received 13 November 2020; Received in revised form 13 January 2021; Accepted 15 January 2021

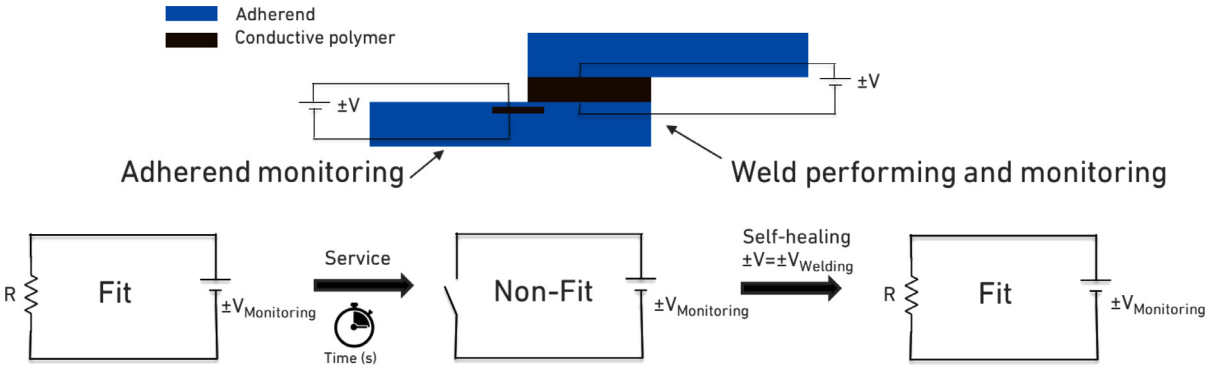

Fig. 1. Concept of welding and self-healing using AM conductive material and embedded circuits.

and addressing the limited building rate of AM process by performing multiple parallel builds.

While fastening and snap-fit connections represent commonly encountered solutions for this issue, the use of adhesive bonding has been explored by several authors (Frascio et al., 2020), as it provides a better distributed stress field that allows for higher joint performance and a larger degree of geometrical freedom in the design of the coupling interfaces. Furthermore, a locally controlled, AM-enabled tailoring of the mechanical properties is leading towards the implementations of graded and functionally graded structures and bondline (Nakanouchi et al., 2019, dos Reis et al., 2020), to change the joint stress distribution, e.g. reducing peel stress at overlap ends, addressing some of the major drawbacks of the bonding technology (da Silva et al., 2018). Moreover, DfAM could allow to obtain AM components ready to be assembled by the AM-enabled control on the material properties, on the surfaces patterns or using integrated material treatments in the AM build, e.g. plasma treatment can be integrated in the materials deposition to improve intralayer adhesion (Frascio et al., 2020).

Considering most AM processes rely on thermoplastic polymers, other joining processes are also suitable, mostly based on thermal welding, many of which have already been found to be effective for joining long fibre thermoplastic matrix reinforced materials (Ahmed et al., 2006). Moreover, implementing DfAM for these processes can further explore the advantages of multi material additive manufacturing MMAM to include conductive reinforced polymers and direct writing (Wang et al., 2020, Kwok et al., 2017, Flowers et al., 2017, Mora et al., 2020, Stano et al., 2020) to embed circuits and heating elements through the thickness of the materials. The end result are components that can be joined together via the application of a controlled electric current. Other key advantages are the geometrical freedom obtainable in the weld zone, as no access for external tools is needed, and the improved control over the welding set up geometry, one of the most relevant process parameters (Brassard et al., 2020). Furthermore, these circuits and heating elements could also be used for structural monitoring and to enable self-healing (Fig. 1), taking advantage of the knowledge on the failure mechanism of layered materials developed on components manufactured with other processes (Banea and Da Silva, 2009, Shang et al., 2019).

Finally, taking in account the layered nature of AM processed materials and the current state of the art in bonding and welding joining processes, the use of AM opens the possibility to design and manufacture novel energy absorbing and crashworthy components. These components can combine different joining methodologies to enhance joint performance both under static and dynamic loading conditions (Machado et al., 2018, Braga et al., 2016), redistributing the loads.

In this work an experimental study is carried out on three different joining solutions, suitable for joining AM components. Bonded, welded and hybrid weld-bonded joints are studied. This work was carried out in order to assess the technical feasibility of the different welding and hybrid processes using AM processed conductive thermoplastic filaments and to compare the relative advantages and disadvantages of the different joining solutions.

Table 1
Manufacturing parameters employed in the FFF process.

Printing parameters	
Layer height (mm)	0.2
Infill (%)	100
Deposition speed (mm/s)	60
Deposition pattern	lines
Nozzle temperature (°C)	220

2. Materials and methods

In this section the materials used in this work are reported and the characterization methods implemented to carry out the experimental tests are described in detail.

2.1. Materials

An Ender 3 pro 3D printer (Creality, Shenzhen, China), equipped with 0.4 mm nozzle was used for the fabrication of the adherends using a Fused Filament Fabrication (FFF) process. Two different polylactic acid (PLA) thermoplastic filaments were used, a bulk PLA by Sunlu for the adherends (Zhuhai sunlu industrial Co., Zhunhai, China) and a conductive PLA by ProtoPasta for the weld pads (ProtoPlant extrusion technology, Vancouver, Washington, USA). The conductive PLA was selected following the findings of Flowers et al. (Flowers et al., 2017), which reports this material as suitable to manufacture resistors that could be used even to perform welding via joule heating. This is due to the relatively high resistivity ρ of the material, that is equal to 12 Ω cm. The printing parameters reported in Table 1 were used to manufacture the adherends. The mechanical properties of both PLA materials were characterized by manufacturing tensile specimens according to the ASTM D638 – 14, geometry type IV, with the printing set-up used for the adherends (Table 1) and selected according to the manufacturer specifications and to the work by Frascio et al. (Frascio et al., 2019). The specimens were modelled in Creo Parametric 5.0 while the slicing was performed with Ultimaker Cura 4.6, imposing a correction factor to improve dimensional accuracy.

All specimens were manufactured in the same position on the bed, aiming to enhance reproducibility, laid flatwise with crisscross material deposition ± 45° in the raster in respect to the loading direction, as shown in Fig. 2, selected according to the works of Kiendl et al. (Kiendl and Gao, 2020) and Frascio et al. (Frascio et al., 2020), (Frascio et al., 2018). Tensile test with unidirectional material deposition of 0° specimens were performed to obtain the nominal stress to

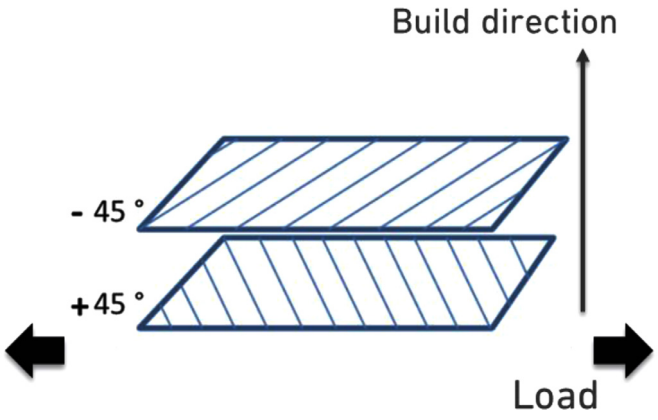

Fig. 2. Material deposition pattern of the specimens.

implement the cohesive law. After manufacturing, the adherends were degreased using isopropyl alcohol, wiping along the main direction.

The adhesive used in this work was the Teroson PU9225 by Henkel (Henkel Italia Srl, Milan, Italy), a bicomponent polyurethane based adhesive, selected due to its mechanical properties, in particular to the adhesive and the PLA Young's modulus ratio, according to the work by Machado et al. (Machado et al., 2018).

2.2. Experimental methods

2.2.1. Adherends characterization

Recent literature at time of writing (Frascio et al., 2020) pointed out how, for bonded joints with AM adherends, surface modifications could be necessary to improve the adhesion. The surface energy evaluation was carried out on the AM adherends, in the overlap area, in order to take into account the effect of the surface morphology created by the manufacturing process (Bergonzi et al., 2021, Packham, 2018). The surface energy was assessed via contact angle measurements, using the equilibrium of the forces, as proposed by Young's equation Gordon (1805) and the Owens-Wendt-Rabel-Kaelble (OWRK) method Owens and Wendt (1969). The contact angle measurements were performed using a OCA 15 goniometer (DataPhysics, Neurtek Instruments, Eibar, Spain) under ambient conditions, using three different liquids: water (polar liquid), ethylene glycol 55% (polar liquid) and n-hexadecane (nonpolar) as shown in (Dantas et al., 2021). The procedure was repeated after an atmospheric pressure plasma (APP) surface treatment. The APP treatment was carried out using Arcotec GmbH (Ebhausen, Germany) equipment, manoeuvring the torch at a distance of 15 mm from the surface for 180 s, the treatment parameters were set according to literature and previous experience of the authors (Dantas et al., 2021, Frascio et al., 2021, Jordá-Vilaplana et al., 2014, Noeske et al., 2004).

2.2.2. Adhesive characterization

Adhesive characterization was performed to produce the data for the finite element analysis (FEA) model of the joint. The Teroson PU9225 adhesive was characterized through bulk tensile test, according to the ASTM D638 – 14, geometry type IV, and by performing Double Cantilever Beam (DCB) and End-Notched Flexure (ENF) tests. The DCB and ENF tests were performed using two different set-up configurations, as shown in Fig. 3.

Dimensions	H (mm)	B (mm)	L (mm)	a_0 (mm)	T (mm)
Steel	12.7	25.0	290.0	45.0	0.3
PLA	10.0	20.0	140.0	30.0	0.3

The first test configuration uses steel adherends and fracture tests were carried out according to the procedure shown in the work by de Moura et al. (de Moura et al., 2008, de Moura et al., 2009). This is a standardized procedure and was performed to obtain results comparable with the ones published in the literature. Compliance-Based Beam Method (CBBM) data reduction was used and critical fracture energy evaluation was done using Eq. (1) for mode I

$$G_{IC} = \frac{6p^2}{B^2 h}\left(\frac{2a_e^2}{h^2 E_f} + \frac{1}{5G_{13}}\right) \quad (1)$$

and using Eq. (2) for mode II

$$G_{IC} = \frac{9p^2 a_e^2}{16B^2 E_f h^3} \quad (2)$$

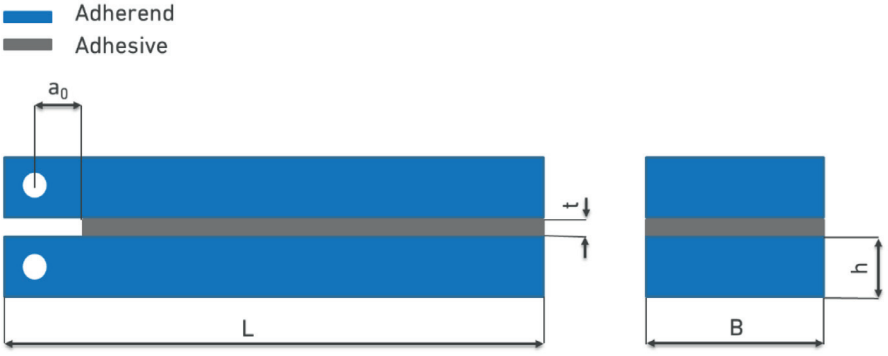

Fig. 3. DCB and ENF nominal dimensions for steel and AM PLA specimens (Bergonzi et al., 2021, de Moura et al., 2008).

Dimensions	h (mm)	B (mm)	L (mm)	a_0 (mm)	t (mm)
Steel	12.7	25.0	290.0	45.0	0.3
PLA	10.0	20.0	140.0	30.0	0.3

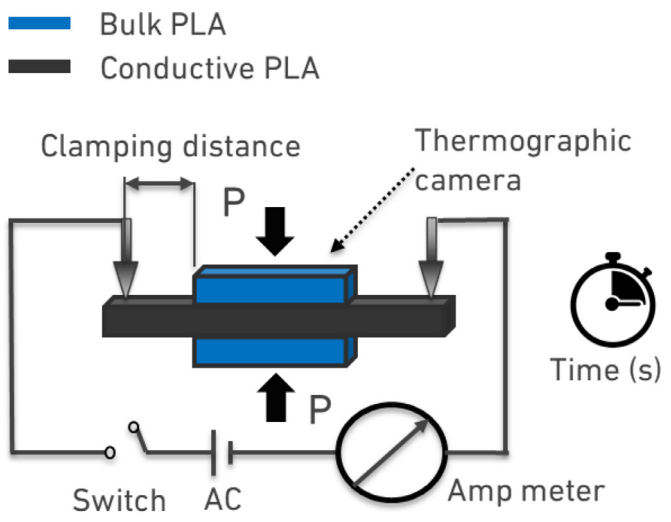

Fig. 4. Welding process set up realized according to (Brassard et al., 2020, Hou et al., 1999).

Where P is the load, a_e is the equivalent crack length to account for the fracture process zone, E_f is the flexural modulus of the adherend, G_{13} is the shear modulus of the adherend, B is the width and h is the height of the adherend (Fig. 3). The second test configuration uses PLA adherends, according to the work by Bergonzi et al. (Bergonzi et al., 2021) for mode I (DCB test), using cylindrical contact points of radius 5 mm and a span of 100 mm for mode II (ENF test), in order to produce representative data of the real joint configuration, being able of taking into account the effect of the AM surface morphology in case of weak adhesion (interfacial failure).

At least three repetitions were performed for each characterization test.

2.2.3. Welding process set-up

The welding set up design, shown in Fig. 4, was based on the works by Hou et al. (1999) and Brassard et al. (2020).

The welding set up comprises of a non-conductive jig, an AC power supply, able to provide up to 220 V at 50 Hz and controlled using pulse-width modulation (PWM), a thermographic camera Fluke Ti25 Thermal Imager (Fluke Ibérica, S.L., Madrid, Spain) and a system to adjust the clamping distance. It is worth noting that clamping distance is one of the most relevant process parameters, as pointed out in (Brassard et al., 2020). The thermal cycle was adjusted in order to obtain a temperature range in the 170–250 °C range in the welding area, as recommended in the work of Vanaei et al. (2021). The welding process parameters were chosen with a preliminary characterization: the configuration used for the joints was modified on the upper side, replacing the full size adherend with a single layer adherend. Using this configuration was possible to measure a thermal map representative of the studied application. A clamping distance of 1.5 mm was selected, for which the resistance of the conductive plates was assessed to be 1.5 ± 0.4 kΩ in between the contact points. The optimum welding parameters were found to correspond to a power density of 440 kW/m^2 and a pressure of 1 MPa applied for a time of 120 s.

2.2.4. Joint configurations

In this work three joint configurations were investigated. These are the bonded, welded and hybrid weld-bonded joints (Fig. 5).

To select the adherend thickness and to determine the adhesive percentage of the total overlap in the hybrid solution, a preliminary linear elastic FEA analysis was carried out with the Abaqus (Dassault Systèmes Simulia Corp., Johnston, Rhode Island, United States) finite element software. An adherend thickness of 8 mm was selected to guarantee stress levels below the PLA yielding value. The adhesive overlap length in the hybrid solution was selected to improve the joints reproducibility and by observing the trend of the maximum peel and shear stresses, which were found to stabilize in the weld for a total bond length greater than 16 mm. The selected joint geometry is reported in Fig. 6 with the same overlap length and bondline thickness being used for all investigated configurations. Bulk PLA thin spacers were 3D printed at conductive PLA ends to ease the joint manufacturing process and shield the adhesive during the welding process.

All mechanical characterization processes were performed using a universal testing machine, the INSTRON® 3367 (Norwood, Massachusetts, USA) equipped with a 30 kN load cell. The tests were carried out under displacement control and at a test speed of 1 mm/min. Load-displacement (P- δ) curves were obtained for each configuration and at least three repetitions were performed for each characterization test.

3. Numerical modelling

A finite element analysis (FEA) was performed using the Abaqus finite element software package for the bonded, welded and weld bonded joint configurations under study (Fig. 7).

All the experiments were 2D modelled with plain strain, four node, quadrilateral solid elastic elements (type CPE4) for the adherends and the adhesive or the weld. In the bondline, a cohesive layer of 0.1 mm was modelled using four node cohesive elements (COH2D4). The layer of cohesive elements is implemented with a triangular traction-separation

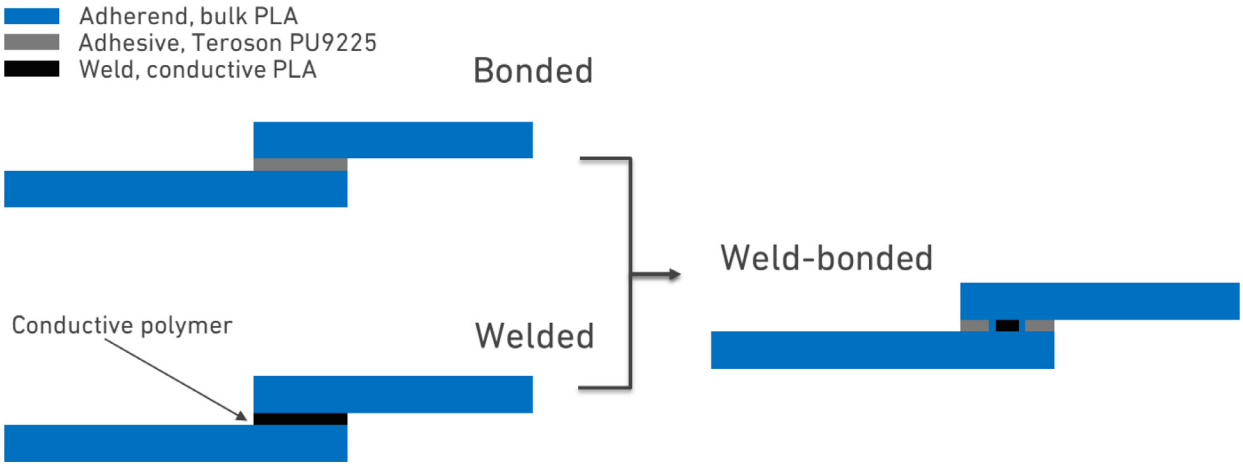

Fig. 5. Joints configurations investigated.

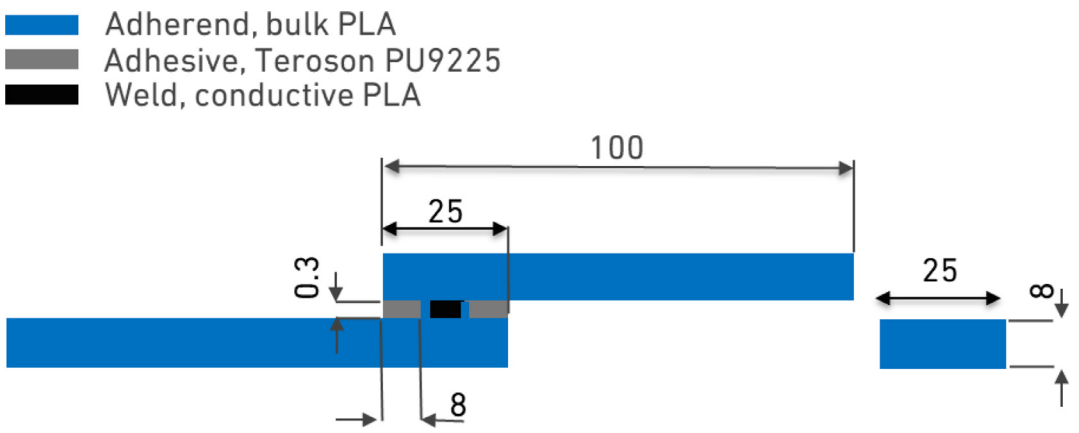

Fig. 6. Joints geometry dimensions (expressed in mm).

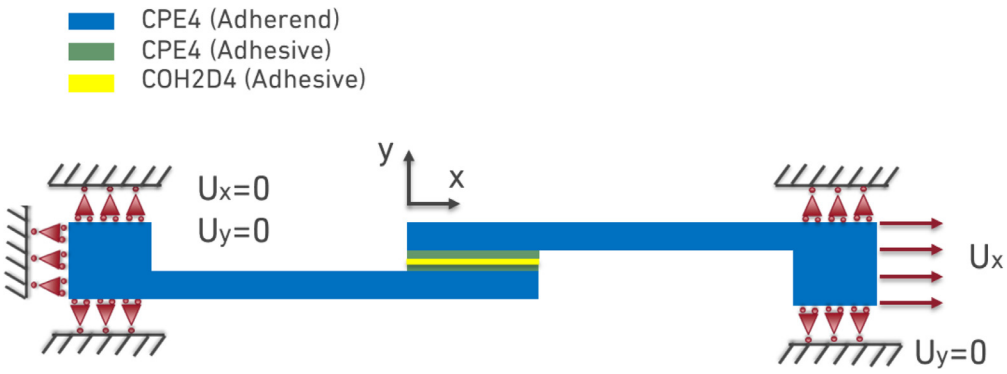

Fig. 7. Schematic representation of the numerical model realized in Abaqus for the bonded, welded and weld bonded joint configurations.

Table 2
Bulk and conductive PLAs mechanical properties

	Young's modulus (MPa)	Stress at failure (MPa)	Strain at failure (%)
Bulk PLA	2850.4	56.4	3.4
Standard deviation	46.8	2.1	0.17
Conductive PLA	3110.5	54.5	2.4
Standard deviation	134.7	4.4	0.18

cohesive zone model (CMZ) law using the values obtained as reported in 2.2.2 section, allowing to accurately model the joint failure process. The dependence of the fracture energy on the mixed mode was modelled using the power law fracture criterion. The mesh size was refined to reduce element size in areas where large stress gradient occurs correspond and to ensure at least five cohesive elements within the fracture process zone at incipient failure. Each section of the model was assigned with the material properties obtained in the experimental characterization of the materials, described in Section 2.

4. Results and discussion

4.1. Polylactic acid characterization

The results of the mechanical characterization of the PLA materials are reported in Table 2. It is worth noting that the stiffnesses of the bulk PLA and the conductive PLA differ by less than 10%, a result consistent to what is reported by Rane et al. (2019). Therefore, it could be possible to tailor the physical properties for the specific application, using the conductive particles as explored in (Wang et al., 2020, Kolisnyk et al., 2019), without creating significant stiffness gradients in the component that could result in undesirable stress intensity factor effect under service loads.

The unidirectional specimens stress at failure was 26.2 ± 1.5 MPa, this value was used to model the welded material strength in the cohesive law as representative of the intralayer adhesion between the fused filaments.

The PLA surface energy characterization identified an increase of the surface energy from 33.3 mJ/m^2 (as is from 3D printing) to 61.1 mJ/m^2 (after APP treatments). The typical contact angles obtained with water droplets are shown in Fig. 8.

Fig. 8: Typical contact angle for wated droplet on AM PLA surface (a) as is from manufacturing, 77º±1º; (b) after 180 s of APP surface treatment, 40º±1º.

4.2. Adhesive characterization

The results of the tensile test on the Teroson PU9225 bulk adhesive are reported in Table 3.

The results of the DCB and ENF test, using the Teroson PU9225 adhesive with steel and AM PLA adherends are reported in Table 4.

Although cohesive failure was found in the tests carried out with steel adherends, with the PLA adherends weak adhesion was identified, as the failure surfaces showed a mixed failure mechanism, despite the APP surface treatment (Fig. 9).

As cohesive failure corresponds to the maximum performance achievable in the bondline (da Silva et al., 2018), by comparing the

Table 3
Tensile mechanical properties of bulk Teroson PU9225 adhesive.

	Young's Modulus (MPa)	Stress at failure (MPa)	Strain at failure (%)
Average	576.9	13.3	13.0
Standard deviation	16.1	0.3	0.1

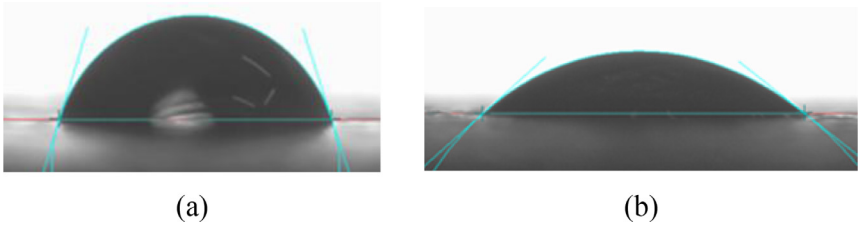

Fig. 8. Representative fracture surfaces for steel adherends (a) and PLA adherends (b) obtained performing DCB tests according to (Bergonzi et al., 2021, de Moura et al., 2008).

Fig. 9. Representative experimental curve and FEA result for the bonded SLJ.

Table 4
Adhesive and cohesive characterization of the Teroson PU9225 adhesive.

	STEEL	PLA
Fracture toughness mode I	G_{IC} (N/mm)	G_{IC} (N/mm)
Average	1.39	0.53
Standard deviation	0.04	0.15
Fracture toughness mode II	G_{IIC} (N/mm)	G_{IIC} (N/mm)
Average	7.60	1.90
Standard deviation	0.10	0.14
Failure	Cohesive	Mixed

values it can be assumed that the bonded joint performance could be improved by exploring different surface modifications, fully integrated in the AM process, e.g. as described in (Frascio et al., 2020), or performed manually, e.g. chemical etching (Dantas et al., 2021).

4.3. Joints test and results comparison

A representative load-displacement curve of the adhesively bonded SLJs is reported in Fig. 9, average failure load was 2722.7±192.8 N.

In Fig. 10 the failure surface of a bonded SLJ is shown, where a mixed failure mechanism can be clearly observed.

Fig. 9 also includes the result from the FEA analysis carried out as described in Section 3 using the cohesive traction-separation law parameters obtained with the PLA adherends (Table 3 and Table 4). A good correlation with the experimental values can be observed.

A representative load-displacement curve of the welded SLJ is reported in Fig. 11, average failure load was 3830.3±177.9 N.

In Fig. 12 a failure surface for the welded SLJ is shown. It can be seen that failure is cohesive in the weld material.

In Fig. 11 the load-displacement curve obtained with the FEA model is also reported. The cohesive traction-separation law was fitted using the parameters ranges suggested in literature (Spoerk et al., 2017, Khan et al., 2019). Good correlation was found by setting G_{IC} equal to 0.4 N/mm and G_{IIC} equal to 0.8 N/mm.

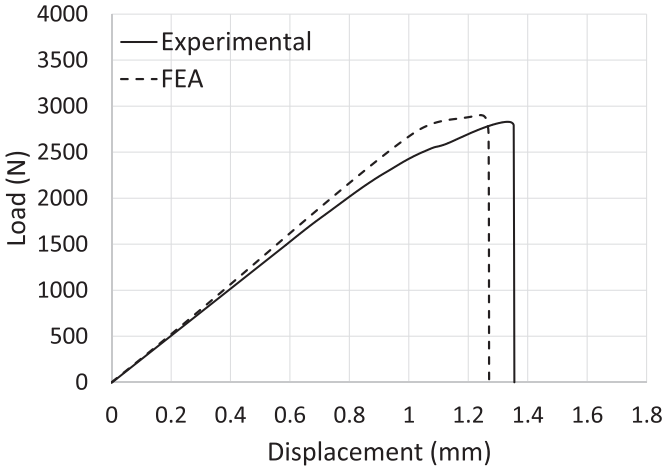

Fig. 10. Typical failure surface for adhesively bonded SLJ, nominal bonding area is 25x25 mm.

A representative load-displacement curve of the weld-bonded SLJ is reported in Fig. 13 average failure load was 2777.5 ± 232.9 N. Around 0.9 mm of displacement a drop in load can be observed; by visual inspection of the specimens while performing the joint tests was possible to notice that it is correlated to a first failure that occurs in the bonded overlap of the hybrid weld-bonded joint..

Observing the failure surface of an hybrid joint, shown in Fig. 14, it can be seen as the adhesive is not affected by the different joint configuration, while the weld failure process is slightly different, suggesting that this process output is geometry dependent (Brassard et al., 2020).

The FEA model is implemented using the CMZ traction-separation laws validated for the bonded and welded SLJ configurations (Moroni et al., 2010). It can be observed how the model is able to provide a good agreement with the experimental data in the elastic portion of the curve, while, at failure, load and displacement are both overestimated. In Fig. 13 it is shown how the FEA model result diverges from

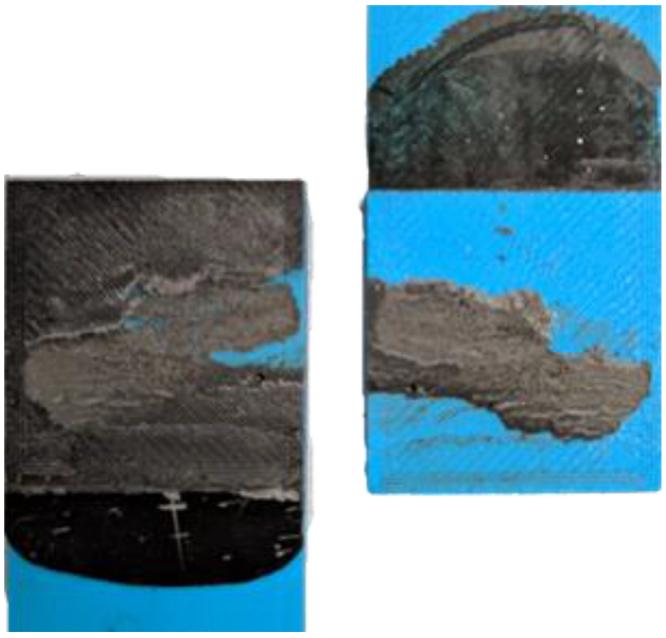

Fig. 11. Representative experimental curve and FEA result for the welded SLJ.

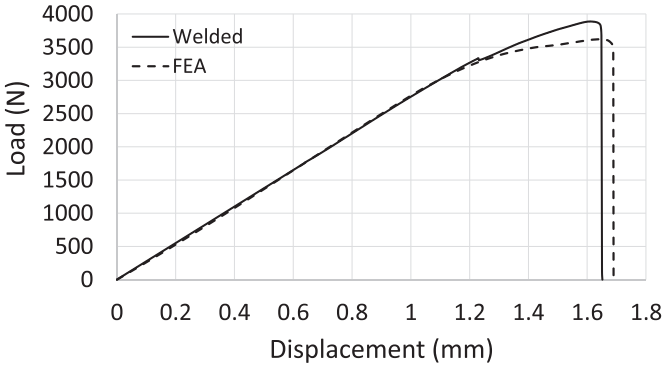

Fig. 12. Typical failure surface for welded SLJ, nominal welding area is 25x25 mm.

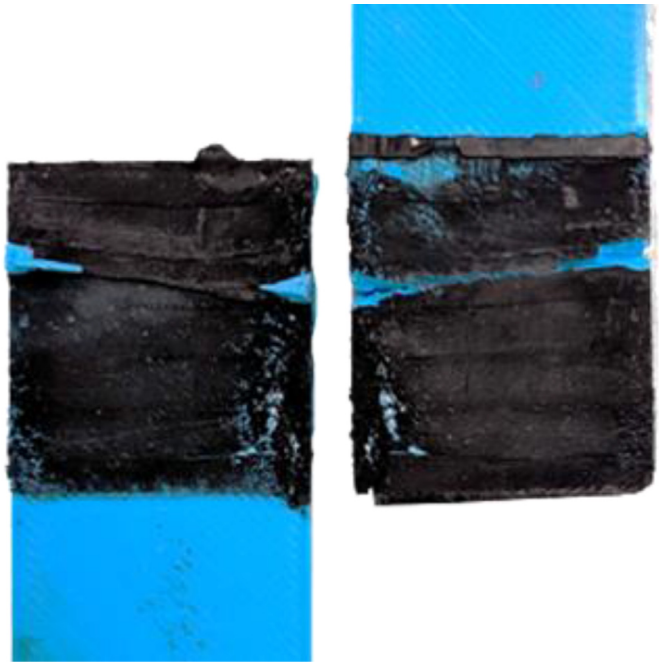

Fig. 13. Representative experimental curve and FEA result s for the weld-bonded SLJ.

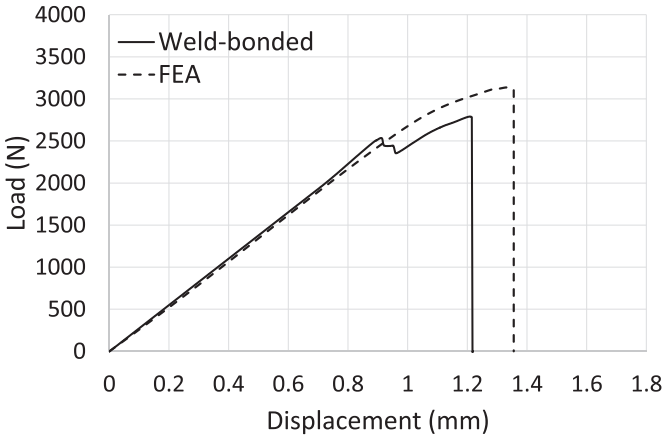

Fig. 14. Typical failure surface for weld-bonded SLJ, nominal joining area is 25x25 mm.

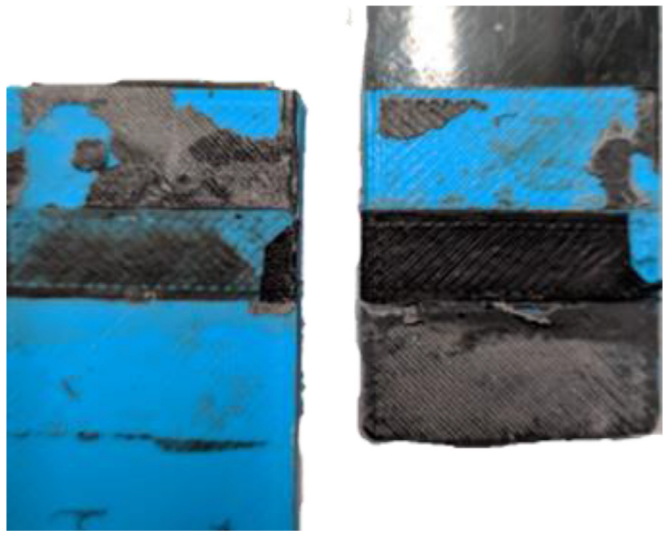

Fig. 15. Comparison of the representative experimental curves of the investigated SLJ configurations.

the experimental one at the displacement that corresponds to the failure in the adhesive despite the same fracture pattern can be observed in the experiment and in the numerical model, that is at first in the bonded areas of the overlap and then in the welded notch. This difference can be related to the approximations of the inverse method used to model the weld-bonded joint due to its performance geometry dependency and to the mixed-mode of failure of the adhesive.

A comparison of the experimental results for all the investigated configurations is shown in Fig. 15 superimposing the representative curves.

It can be seen that in the explored configurations the welded SLJ has the best performance in terms of load and displacement, while the hybrid weld-bonded configuration has similar performance to the bonded joint in terms of maximum load.

5. Conclusions

An experimental study on three different joining solutions for AM materials was carried out, considering bonded, welded and weld-bonded joints. A dedicated set-up for the welding process was designed and a preliminary characterization process was performed to determine the process parameters that lead to cohesive failure of the joint. The effectiveness of the APP surface treatment procedure was assessed through surface energy measurement and this technique was used to improve the adhesion in bonded and weld-bonded joints. SLJs were mechanically

tested for each joining solution and corresponding numerical models were developed in order to better understand the performance of each configuration under study.

- Adhesive bonding of AM processed components is a challenging process due to the low surface energy of thermoplastic polymers and the peculiar morphology conferred by the material deposition pattern. Thus, 3D printing parameters and component positioning should be considered as major joint design factors. For the materials used in this work, weak adhesion was encountered even after APP surface treatment. This indicates that alternative surface treatment solutions, e.g. chemical etching, should be explored to enable structural applications of this joining process.
- The technical feasibility of the hybrid weld-bonded joint using AM with a conductive thermoplastic polymer was assessed and a corresponding numerical model was created. This model was able to show good correlation with the experimental results. The investigated configuration, both in terms of materials and geometry, did not lead to a performance improvement. This was mainly a result of the low level of adhesion between the adhesive and the AM substrates. Hybrid weld-bonded joints and bonded joints with stiffness tailored bondline solutions were proven to be effective after geometry optimization and especially under dynamic loading conditions. The obtained results suggest that this joining solution, with further optimizations to the adhesion level, will be relevant for industrial applications for component manufactured with AM and composed of long fibre reinforced thermoplastic matrices.
- The welding joining process was found to be a highly promising joining process for the assembly of AM components. No surface modification was required for the proposed configuration and, taking advantage of multi material AM process capability for direct printing of integrated circuits, it is entirely possible to design components ready to be assembled and with an optimized geometry of the welding area. It is worth noting that integrating welding setup in the component would ease the welding process, overcoming critical aspects such as the need for a fine control over the clamping distance. Theoretically, any polymer can be used with conductive particles and multi material AM can be used to create joints with tailored stiffness, achieved by varying the volumetric percentage of the reinforcements and the matrix polymers.

Finally, the results of this work clearly indicate that locally controlled joule heating using AM with a conductive thermoplastic filament could be expanded to other joint designs, such as locally cured adhesives (using conductive pads at adherend-adhesive interface), or self-healing (placing conductive pads in critical area were delamination and damage could occur). These features can all be implemented with the inclusion of dedicated embedded circuits in the bulk material, able to perform localized welding through the thickness.

Declaration of Competing Interest

None.

References

Han, D, Lee, H., 2020. Recent advances in multi-material additive manufacturing: methods and applications. Curr. Opin. Chem. Eng. 28, 158–166. doi:10.1016/j.coche.2020.03.004.

Tan, LJ, Zhu, W, Zhou, K., 2020. Recent progress on polymer materials for additive manufacturing. Adv. Funct. Mater. 30, 2003062. doi:10.1002/adfm.202003062.

Arif, MF, Alhashmi, H, Varadarajan, KM, Koo, JH, Hart, AJ, Kumar, S., 2020. Multifunctional performance of carbon nanotubes and graphene nanoplatelets reinforced PEEK composites enabled via FFF additive manufacturing. Compos. Part B Eng. 184, 107625. doi:10.1016/j.compositesb.2019.107625.

van de Werken, N, Tekinalp, H, Khanbolouki, P, Ozcan, S, Williams, A, Tehrani, M., 2020. Additively manufactured carbon fiber-reinforced composites: State of the art and perspective. Addit Manuf. 31, 100962. doi:10.1016/j.addma.2019.100962.

Ramola, M, Yadav, V, Jain, R., 2019. On the adoption of additive manufacturing in healthcare: a literature review. J. Manuf. Technol. Manag. 30, 48–69. doi:10.1108/JMTM-03-2018-0094.

Ghomi, ER, Khosravi, F, Neisiany, RE, Singh, S, Ramakrishna, S., 2020. Future of additive manufacturing in healthcare. Curr. Opin. Biomed. Eng., 100255 doi:10.1016/j.cobme.2020.100255.

Jilich, M, Frascio, M, Avalle, M, Zoppi, M., 2019. Development of a gripper for garment handling designed for additive manufacturing. Proc. Inst. Mech. Eng. Part C J. Mech. Eng. Sci. 0, 1–12. doi:10.1177/0954406219857763.

Kaur, M, Kim, WS., 2019. Toward a smart compliant robotic gripper equipped with 3D-designed cellular fingers. Adv. Intell. Syst. 1, 1900019. doi:10.1002/aisy.201900019.

Zaharia, SM, Enescu, LA, Pop, MA., 2020. Mechanical Performances of Lightweight Sandwich Structures Produced by Material Extrusion-Based Additive Manufacturing. Polymers (Basel) 12, 1740. doi:10.3390/polym12081740.

Özen, İ, Çava, K, Gedikli, H, Alver, Ü, Aslan, M., 2020. Low-energy impact response of composite sandwich panels with thermoplastic honeycomb and reentrant cores. Thin-Walled Struct. 156, 106989. doi:10.1016/j.tws.2020.106989.

Mao, Y, Wu, L, Yan, DM, Guo, J, Chen, CW, Chen, B., 2018. Generating hybrid interior structure for 3D printing. Comput. Aided Geom Des. 62, 63–72. doi:10.1016/j.cagd.2018.03.015.

de Lima, CR, Paulino, GH., 2019. Auxetic structure design using compliant mechanisms: a topology optimization approach with polygonal finite elements. Adv. Eng. Softw. 129, 69–80. doi:10.1016/j.advengsoft.2018.12.002.

Ahmed, K, Shiblee, MNI, Khosla, A, Nagahara, L, Thundat, T, Furukawa, H., 2020. Review—recent progresses in 4D printing of gel materials. J. Electrochem. Soc. 167, 037563. doi:10.1149/1945-7111/ab6e60.

Alfaify, A, Saleh, M, Abdullah, FM, Al-Ahmari, AM., 2020. Design for additive manufacturing: a systematic review. Sustainability 12, 7936. doi:10.3390/su12197936.

Wood, BM., 2016. Design and Manufacture for Multifunctionality - 5 Multifunctionality in Additive Manufacturing. Elsevier Inc. doi:10.1016/B978-0-323-34061-8/00005-3.

Wang, J, Mubarak, S, Dhamodharan, D, Divakaran, N, Wu, L, Zhang, X., 2020. Fabrication of thermoplastic functionally gradient composite parts with anisotropic thermal conductive properties based on multicomponent fused deposition modeling 3D printing. Compos. Commun. 19, 142–146. doi:10.1016/j.coco.2020.03.012.

Bardiya, S, Jerald, J, Satheeshkumar, V, 2020. Effect of process parameters on the impact strength of fused filament fabricated (FFF) polylactic acid (PLA) parts.. Mater Today Proc doi:10.1016/j.matpr.2020.08.066.

Bergonzi, L, Pirondi, A, Moroni, F, Frascio, M, Avalle, M., 2021. A study on fused filament fabrication (FFF) parameters as bonded joint design factors. J. Adhes.

Frascio, M, Bergonzi, L, Jilich, M, Moroni, F, Avalle, M, Pirondi, A, et al., 2019. Additive manufacturing process parameter influence on mechanical strength of adhesive joints, preliminary activities. Acta Polytech. CTU Proc. 25, 41–47. doi:10.14311/APP.2091.25.0041.

Kiendl, J, Gao, C., 2020. Controlling toughness and strength of FDM 3D-printed PLA components through the raster layup. Compos. Part B Eng. 180, 107562. doi:10.1016/j.compositesb.2019.107562.

Chacón, JM, Caminero, MA, Núñez, PJ, García-Plaza, E, García-Moreno, I, Reverte, JM., 2019. Additive manufacturing of continuous fibre reinforced thermoplastic composites using fused deposition modelling: effect of process parameters on mechanical properties. Compos. Sci. Technol. 181, 107688. doi:10.1016/j.compscitech.2019.107688.

Frascio, M, Marques EA de, S, Carbas, RJC, da Silva, LFM, Monti, M, Avalle, M., 2020. Review of tailoring methods for joints with additively manufactured adherends and adhesives.. Materials (Basel) 13, 3949. doi:10.3390/ma13183949.

Nakanouchi, M, Sato, C, Sekiguchi, Y, Haraga, K, Uno, H., 2019. Development of application method for fabricating functionally graded adhesive joints by two-component acrylic adhesives with different elastic moduli. J. Adhes 95, 529–542. doi:10.1080/00218464.2019.1583562.

dos Reis, MQ, Carbas, RJ, Marques, EA, da Silva, LF., 2020. Numerical modelling of multi-material graded joints under shear loading. Proc. Inst. Mech. Eng. Part E J. Process Mech. Eng. 0, 095440892091611. doi:10.1177/0954408920916112.

da Silva, LFM, Öchsner, A, Adams, RD, 2018. Handbook of Adhesion Technology. Cham: Springer International Publishing doi:10.1007/978-3-319-55411-2.

Ahmed, TJ, Stavrov, D, Bersee, HEN, Beukers, A., 2006. Induction welding of thermoplastic composites—an overview. Compos. Part A Appl. Sci. Manuf. 37, 1638–1651. doi:10.1016/j.compositesa.2005.10.009.

Kwok, SW, Goh, KHH, Tan, ZD, Tan, STM, Tjiu, WW, Soh, JY, et al., 2017. Electrically conductive filament for 3D-printed circuits and sensors. Appl. Mater. Today 9, 167–175. doi:10.1016/j.apmt.2017.07.001.

Flowers, PF, Reyes, C, Ye, S, Kim, MJ, Wiley, BJ., 2017. 3D printing electronic components and circuits with conductive thermoplastic filament. Addit Manuf. 18, 156–163. doi:10.1016/j.addma.2017.10.002.

Mora, A, Verma, P, Kumar, S., 2020. Electrical conductivity of CNT/polymer composites: 3D printing, measurements and modeling. Compos Part B Eng 183, 107600. doi:10.1016/j.compositesb.2019.107600.

Stano, G, Di Nisio, A, Lanzolla, A, Percoco, G., 2020. Additive manufacturing and characterization of a load cell with embedded strain gauges. Precis Eng. 62, 113–120. doi:10.1016/j.precisioneng.2019.11.019.

Brassard, D, Dubé, M, Tavares, JR., 2020. Modelling resistance welding of thermoplastic composites with a nanocomposite heating element. J. Compos. Mater. doi:10.1177/0021998320957055.

Banea, MD, Da Silva, LFM, 2009. Adhesively bonded joints in composite materials: an overview. Proc. Inst. Mech. Eng. Part L J. Mater. Des Appl 223, 1–18. doi:10.1243/14644207JMDA219.

Shang, X, Marques, EAS, Machado, JJM, Carbas, RJC, Jiang, D, da Silva, LFM., 2019. Review on techniques to improve the strength of adhesive joints with composite adherends. Compos Part B Eng 177, 107363. doi:10.1016/j.compositesb.2019.107363.

Machado, JJM, Gamarra, PMR, Marques, EAS, da Silva, LFM., 2018. Improvement in impact strength of composite joints for the automotive industry. Compos Part B Eng 138, 243–255. doi:10.1016/j.compositesb.2017.11.038.

Braga, DFO, De Sousa, LMC, Infante, V, Da Silva, LFM, Moreira, PMGP, 2016. Aluminium friction-stir weld-bonded joints. J Adhes 92, 665–678. doi:10.1080/00218464.2015.1085860.

Frascio, M, Avalle, M, Monti, M., 2018. Fatigue strength of plastics components made in additive manufacturing: First experimental results. Proc. Struct. Integr. 12, 32–43. doi:10.1016/j.prostr.2018.11.109.

Packham, DE., 2018. Theories of fundamental adhesion. Handb. Adhes. Technol. Second Ed. vol. 1–2, 11–41. doi:10.1007/978-3-319-55411-2_2.

Gordon, IRF., 1805. An essay on the cohesion of fluids. Philos. Trans. R Soc. London 95, 65–87. doi:10.1098/rstl.1805.0005.

Owens, DK, Wendt, RC., 1969. Estimation of the surface free energy of polymers. J. Appl. Polym Sci. 13, 1741–1747. doi:10.1002/app.1969.070130815.

Dantas, MA, Carbas, RJ, Marques, EAS, Kushner, D, Silva, LFM., 2021. Flexible tubular metal-polymer adhesive joints under torsion loading. Int. J. Adhes. Adhes 104–125.

Frascio, M, Mandolfino, C, Moroni, F, Jilich, M, Lagazzo, A, Pizzorni, M, et al., 2021. Appraisal of surface preparation in adhesive bonding of additive manufactured substrates. Int. J. Adhes. Adhes, 102802 doi:10.1016/j.ijadhadh.2020.102802.

Jordá-Vilaplana, A, Fombuena, V, García-García, D, Samper, MD, Sánchez-Nácher, L., 2014. Surface modification of polylactic acid (PLA) by air atmospheric plasma treatment. Eu. Polym. J. 58, 23–33. doi:10.1016/j.eurpolymj.2014.06.002.

Noeske, M, Degenhardt, J, Strudthoff, S, Lommatzsch, U., 2004. Plasma jet treatment of five polymers at atmospheric pressure: surface modifications and the relevance for adhesion. Int. J. Adhes. Adhes. 24, 171–177. doi:10.1016/j.ijadhadh.2003.09.006.

de Moura, MFSF, Campilho, RDSG, Gonçalves, JPM., 2008. Crack equivalent concept applied to the fracture characterization of bonded joints under pure mode I loading. Compos. Sci. Technol. 68, 2224–2230. doi:10.1016/j.compscitech.2008.04.003.

de Moura, MFSF, Campilho, RDSG, Gonçalves, JPM., 2009. Pure mode II fracture characterization of composite bonded joints. Int. J. Solids Struct. 46, 1589–1595. doi:10.1016/j.ijsolstr.2008.12.001.

Hou, M, Ye, L, Mai, YW., 1999. An experimental study of resistance welding of carbon fibre fabric reinforced polyetherimide (CF Fabric/PEI) composite material. Appl. Compos. Mater. 6, 35–49. doi:10.1023/A:1008879402267.

Vanaei, HR, Shirinbayan, M, Costa, SF, Duarte, FM, Covas, JA, Deligant, M, et al., 2021. Experimental study of PLA thermal behavior during fused filament fabrication. J. Appl. Polym. Sci. 138, 1–7. doi:10.1002/app.49747.

Rane, A.V., Kanny, K, Mathew, A, Mohan, TP, Thomas, S., 2019. Comparative analysis of processing techniques' effect on the strength of carbon black (N220)-filled poly (Lactic Acid). Compos. Strength Mater 51, 476–489. doi:10.1007/s11223-019-00093-6.

Kolisnyk R, Korab M, Iurzhenko M, Masiuchok O, Shadrin A, Mamunya Y, et al. Conductive polymer nanocomposites for novel heating elements, 2019, p. 215–24. https://doi.org/ 10.1007/978-981-13-6133-3_22.

Spoerk, M, Arbeiter, F, Cajner, H, Sapkota, J, Holzer, C., 2017. Parametric optimization of intra- and inter-layer strengths in parts produced by extrusion-based additive manufacturing of poly(lactic acid). J. Appl. Polym. Sci. 134, 45401. doi:10.1002/app.45401.

Khan, AS, Ali, A, Hussain, G, Ilyas, M., 2019. An experimental study on interfacial fracture toughness of 3-D printed ABS/CF-PLA composite under mode I, II, and mixed-mode loading. J. Thermoplast Compos. Mater., 089270571987486 doi:10.1177/0892705719874860.

Moroni, F, Carboni, M, Pirondi, A., 2010. Cohesive zone modelling of 6022-t4 aluminium alloy usmwbonded hybrid joints quasi-static failure. Proc. 18th Eur. Conf. Fract 1–8.